Inorganic Chemistry



pubs.acs.org/IC
Article

# Solvation Structure of $Ag^+$ in 1-Butyl-3-methylimidazolium Bis(trifluoromethylsulfonyl)imide Ionic Liquid: Evidence for Linear *N*-Bound Coordination

Matteo Busato, Martina Sanadar, Paola D'Angelo, and Andrea Melchior*

Cite This: *Inorg. Chem.* 2026, 65, 14023−14032
Read Online



**ABSTRACT:** The coordination environment of the $Ag^+$ ion in the 1-butyl-3-methylimidazolium bis(trifluoromethylsulfonyl)imide ($[C_4mim][Tf_2N]$) ionic liquid (IL) was investigated through a combined experimental and theoretical approach including Raman and Fourier transform-infrared (FT-IR) spectroscopy, density functional theory (DFT) calculations, and X-ray absorption spectroscopy. Raman spectra in the 720−780 $cm^{-1}$ region show the progressive conversion of "free" to coordinated $[Tf_2N]^-$ anions upon addition of the silver salt to $[C_4mim][Tf_2N]$, and quantitative analysis indicates an average coordination number of approximately two anions per $Ag^+$ ion. DFT calculations on the possible coordination isomers of the $[Ag(Tf_2N)_2]^-$ complex reveal that the most stable species consists of two monodentate $[Tf_2N]^-$ ligands bound to the $Ag^+$ cation through the central nitrogen atom, in agreement with the characteristic shifts observed in the experimental FT-IR spectra. Extended X-ray absorption fine structure analysis supports the presence of a well-defined first coordination shell featuring two Ag−N interactions at 2.23(2) Å arranged in an almost linear N−Ag−N geometry. Overall, the combined results establish a predominantly linear, *N*-bound solvation motif for $Ag^+$ in $[C_4mim][Tf_2N]$. This behavior contrasts with the coordination observed in other ILs and highlights the strong influence of the anion on metal ion solvation in these media.

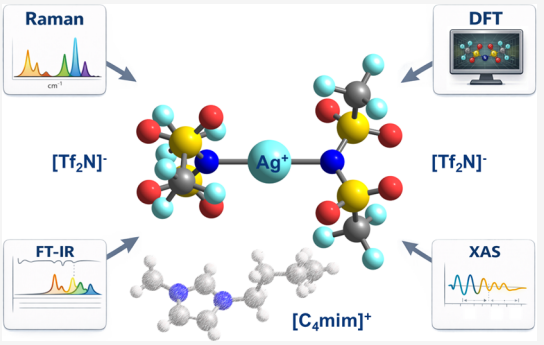


## INTRODUCTION

Over the past decades, ionic liquids (ILs) have attracted considerable interest as alternative solvents owing to their negligible vapor pressure, nonflammability, high thermal and electrochemical stability, and remarkable solvating ability.[1] These features have enabled their application in areas such as selective extraction processes,[2−6] energy storage devices,[7−10] electrodepositions,[11−13] and catalysis.[14,15] In many of these contexts, metal salts are present as dissolved species in the IL phase, making the understanding of metal ion speciation and coordination structure a key issue for controlling reactivity, thermodynamic stability, and transport properties in these media.[16−23]

Among transition metals, silver holds particular technological relevance, and ILs have therefore been explored for the selective recovery of $Ag^+$ from complex aqueous matrices[24−28] as well as for electrodeposition processes of this metal.[12,29−31] Solutions of $Ag^+$ salts in ILs have been extensively investigated for selective olefin/alkane separation, a key step in hydrocarbon processing,[32] exploiting the ability of $Ag^+$ to selectively and reversibly bind olefins through $\pi$-complexation.[33−36] However, despite this technological importance, the structural characterization of $Ag^+$ in ILs remains significantly less explored than in conventional molecular solvents, whereas a clearer description of its solvation structure could support the understanding of the fundamental processes underlying these applications.

In conventional solvents, $Ag^+$ exhibits a highly flexible coordination chemistry, which has been the subject of numerous structural[37−40] and thermodynamic[41−47] studies. In nonaqueous molecular solvents, $Ag^+$ commonly adopts a tetrahedral coordination geometry,[37,48] while in an aqueous solution, a distorted "2 + 2" structure, intermediate between tetrahedral and linear coordination, has been proposed based on X-ray absorption spectroscopy (XAS), large-angle X-ray scattering, and Car−Parrinello molecular dynamics (CPMD) simulations.[37,49] Linear coordination, which is in principle possible due to orbital hybridization promoted by relativistic effects,[50] has also been frequently observed in the presence of *N*-donor ligands in solution,[51,52] highlighting the marked sensitivity of $Ag^+$ coordination to the solvation environment.

Only a limited number of studies have addressed $Ag^+$ solvation in ILs. CPMD simulations on 1-ethyl-3-methylimi-

Received: March 16, 2026
Revised: May 25, 2026
Accepted: June 4, 2026
Published: June 11, 2026

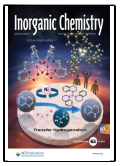





https://doi.org/10.1021/acs.inorgchem.6c01404
*Inorg. Chem.* 2026, 65, 14023−14032

dazolium trifluoromethanesulfonate indicated a disordered and flexible solvation structure with coordination numbers (CNs) ranging from 2 to 5.[53] In *N*-butyl-*N*-methylpyrrolidinium dicyanamide, attenuated total reflectance-ultraviolet spectroscopy, classical molecular dynamics (MD) simulations, and time-dependent density functional theory (DFT) calculations suggested an average of 4.5 anions around $Ag^+$, consistent with a dynamic CN between 4 and 5.[54] More recently, CPMD and XAS investigations on 1-butyl-3-methylimidazolium tetrafluoroborate ($[C_4mim][BF_4]$) demonstrated that $Ag^+$ is coordinated by ~4 $[BF_4]^-$ anions arranged in a roughly tetrahedral geometry.[23] In this system, the coordinated anions were shown to be dynamically exchanging with the bulk IL, giving rise to the $[Ag(BF_4)_4]^{3-} \rightleftharpoons [Ag(BF_4)_3]^{2-} + [BF_4]^-$ equilibrium, while internal anion motions lead to a variable number (4−6) of coordinating fluorine atoms.

Particular attention deserve ILs based on the bis(trifluoromethylsulfonyl)imide anion ($[Tf_2N]^-$). These ILs can achieve high ionic conductivity and marked hydrophobic character, in particular, when paired with an imidazolium cation, making them attractive for electrochemical devices and liquid−liquid biphasic extractions from aqueous media.[7,55,56] From a coordination chemistry perspective, $[Tf_2N]^-$ is known for its structural flexibility and its ability to coordinate metal ions in mono- or bidentate fashion through one or two oxygen atoms belonging to different sulfonyl groups, while coordination through the central nitrogen atom is less common. For divalent transition metal ions, coordination has been shown to occur predominantly via monodentate *O*-binding,[17−20,57] although bidentate modes have also been proposed.[58−62]

For $Ag^+$ in $Tf_2N$-based ILs, however, the structural picture remains controversial. Raman and infrared (IR) spectroscopy studies on silver bis(trifluoromethylsulfonyl)imide ($AgTf_2N$) dissolved in 1-ethyl-3-methylimidazolium bis(trifluoromethylsulfonyl)imide suggested an unusual coordination motif involving two $[Tf_2N]^-$ anions binding via oxygen and one via nitrogen atoms.[63] The simulated vibrational spectra for this structure reproduced the experimental trends satisfactorily. However, alternative coordination motifs were not explored, preventing unambiguous discrimination among possible solvation structures. Coordination of sulfonyl imide anions through nitrogen finds precedent in solid-state structures containing the $[Ag(bis[bis(fluorosulfonyl)imide)]^-$ and $[Ag(bis[bis(methanesulfonyl)amide)]^-$ units.[64,65] Here, the bis(fluorosulfonyl)imide and bis(methanesulfonyl)amide anions, which are structurally analogous to $[Tf_2N]^-$ but bearing −F and $-CH_3$ instead of $-CF_3$ groups, respectively, show coordination to $Ag^+$ via nitrogen atoms in a linear geometry. In the Ag-based IL $[Ag(CH_3CN)_4]_2[Ag(Tf_2N)_3]$, the anionic unit contains $Ag^+$ coordinated by three $[Tf_2N]^-$ ligands via nitrogen atoms.[30] Furthermore, a 2-fold coordination is suggested by electrospray ionization-mass spectrometry of $AgTf_2N$ in 1-butyl-3-methylimidazolium bis(trifluoromethylsulfonyl)imide ($[C_4mim][Tf_2N]$) detecting the $[Ag(Tf_2N)_2]^-$ fragment, although with lower relative intensity compared to the corresponding divalent metal complexes, suggesting a more labile solvation structure for $Ag^+$ in this IL.[60] Such lability may also account for the different solvation thermodynamics shown by $Ag^+$ in ILs compared to other metal ions. While the transfer of divalent metal ions like $Co^{2+}$ and $Zn^{2+}$ from water to $[C_nmim][Tf_2N]$ ($n$ = 2, 4) is a nonspontaneous process,[17,18] $Ag^+$ exhibits a marked different behavior. In particular, its transfer toward $[C_4mim][BF_4]$ was found to be thermodynamically favorable, arising from an enthalpic−entropic balance where a disordered solvation structure and a reduced CN compared to divalent metals play a central role in solvation entropy.[23] Furthermore, transfer-free energies for $Ag^+$ seem to be only slightly unfavorable or even favorable toward $Tf_2N$-based ILs, suggesting a completely different solvation environment compared to divalent metal cations.[23]

In this work, we investigate the coordination environment of the $Ag^+$ ion in $[C_4mim][Tf_2N]$ by combining Raman and Fourier transform-infrared (FT-IR) spectroscopy with XAS and DFT calculations. This integrated experimental−computational approach allowed us to resolve the local structure in the liquid phase and revealed an unusual coordination mode for the $[Tf_2N]^-$ anion, providing new insights into $Ag^+$ speciation in $Tf_2N$-based systems.

## EXPERIMENTAL SECTION

### FT-IR and Raman Spectroscopies

$[C_4mim][Tf_2N]$ (99.5%, water content <100 ppm determined by Karl Fisher titration) and $AgTf_2N$ (99.5%) were purchased from IoLiTec GmbH (Germany) and used without further purification. All solutions were prepared inside a nitrogen-filled glovebox with water content <1 ppm. Samples with different metal salt concentrations were obtained by accurately weighing the required amounts of $AgTf_2N$ and IL. The Ag mole fraction ($x$) was varied in the range $0.0 \leq x \leq 0.40$.

FT-IR spectra were recorded in attenuated total reflectance mode using a Thermo Fisher APEX instrument. Raman spectra were collected in the 100−1700 $cm^{-1}$ range using an Xplora Plus Micro-Raman system (Horiba, Kyoto, Japan) equipped with a 785 nm laser source. The spectra were acquired at room temperature with a spectral resolution of 1 $cm^{-1}$, using 10 accumulations of 20 s and a 50× LWD objective.

The Raman bands associated with free and coordinated $[Tf_2N]^-$ anions were deconvolved and analyzed following procedures previously reported in the literature.[61,66,67] In particular, two bands in the 720−780 $cm^{-1}$ region were used to distinguish between free and bound anions.[66,67] The integrated area of the deconvolved band assigned to the free anion ($I_F$) can be expressed as the product of the molar Raman scattering coefficient ($J_F$) and the molar concentration of free $[Tf_2N]^-$ anion, $C_F$ ($I_F = C_F \cdot J_F$). Similarly, when the Ag mole fraction is used instead of molar concentration, $I_F$ is given by[66]

$$I_F = J'_F \cdot (1 - n \cdot x) \tag{1}$$

where $n$ is the number of coordinated anions and $J'_F$ is the Raman "fractional" scattering coefficient.[66] Then, eq 1 can be rewritten as eq 2, where $I_0$ is the area of the Raman band in the absence of a metal ion:

$$\frac{I_F/I_0}{x} = J'_F \cdot \left(\frac{1}{x} - n\right) \tag{2}$$

The number of coordinating anions $n$ is obtained from linear regression using the slope and intercept parameters.

### DFT Calculations on $Ag^+$ Complexes

DFT calculations were performed using the $\omega$B97XD functional[68] in combination with the def2-TZVP basis set.[69] Geometry optimizations of the 1:2 $[Ag(Tf_2N)_2]^-$ complexes formed between $Ag^+$ and $[Tf_2N]^-$ were first carried out in the gas phase and subsequently within a continuum solvent using the SMD model.[70] The medium effects on the solutes were included by the SMD approach developed to reproduce the solvation free energies of a library of compounds.[71] While this method does not take into account the heterogeneous nature of ILs, it provides a computationally convenient approach to include polarization effects on the solutes demonstrated to provide accurate results in the calculation of thermochemical data in





https://doi.org/10.1021/acs.inorgchem.6c01404
Inorg. Chem. 2026, 65, 14023−14032

solution.[72,73] Vibrational analysis employing the harmonic oscillator approximation was performed for all the obtained minima and showed no imaginary frequencies. Additional geometry optimizations were carried out for the $[Ag(Tf_2N)_2]^-$ complexes including one $[C_4mim]^+$ counterion to include possible many-body effects in vibrational spectra.[63] The $[C_4mim][Tf_2N]$ ionic couple was also optimized at the same level of theory. The coordinates of minimum energy structures are reported in Supporting Information, while the complete vibrational frequencies and oscillator strengths are reported in Table S1. Free energies were calculated by adding to the electronic energy the zero-point vibrational energy (ZPVE) and thermal corrections. All calculations were performed using the Gaussian 16 program Rev. A.03.[74]

### XAS Measurements and Data Analysis

Ag K-edge XAS measurements were performed in transmission mode on a 0.1 mol $L^{-1}$ $AgTf_2N$ solution in $[C_4mim][Tf_2N]$ at the 11.1 XAFS beamline of Elettra−Sincrotrone Trieste (Italy).[75] The liquid sample was loaded into a dedicated cell equipped with Kapton windows and maintained under a continuous nitrogen flux during data acquisition to prevent exposure to atmospheric moisture. Data were collected using a Si(311) double-crystal monochromator, with the storage ring operating at 2 GeV and a beam current between 200 and 300 mA. Energy calibration was performed using a silver metal foil as a reference. Three spectra were recorded and averaged to improve the signal-to-noise ratio.

The extended X-ray absorption fine structure (EXAFS) region of the absorption spectrum was analyzed using the GNXAS program.[76,77] Scattering amplitudes and phase shifts were calculated within the muffin-tin (MT) approximation from clusters of fixed geometry. To this end, the DFT-optimized $[Ag(Tf_2N)_2]^-$ clusters were employed (see above). MT radii were chosen to ensure an ∼20% overlap between adjacent MT spheres and were set to 1.91, 1.00, 0.90, 0.80, 0.80, and 0.70 Å for Ag, S, O, N, C, and F atoms, respectively.[18,23,40] Photoelectron inelastic losses in the final state were taken into account using advanced models for the exchange−correlation self-energy in the Hedin−Lundqvist scheme.[78]

Theoretical signals associated with *n*-body distribution functions were calculated within the multiple-scattering (MS) theory and summed to reconstruct the total theoretical contribution. In a first stage, the analysis was carried out by considering the N2 structure, identified as the most probable coordination in solution (*vide infra*). Accordingly, single-scattering (SS) theoretical signals involving the Ag−N, Ag−S, and Ag−O photoelectron paths were included, together with MS contributions associated with the Ag−N−S and N−Ag−N three-body distributions. The Ag−O path refers to the O atom closest to the photoabsorber. A schematic representation of the SS and MS paths included in the analysis is shown in Figure S1. Initial values for the N−S and S−O distances within the $[Tf_2N]^-$ anion were taken from the DFT-optimized structure (1.63 and 1.45 Å, respectively), as well as the Ag−N−O and N−S−O angles (118° and 108°, respectively), while a collinear configuration was considered for N−Ag−N. Each two-body distribution was modeled as a Γ-like function depending on four structural parameters: the path degeneracy $N$, the average distance $R$, the Debye−Waller factor $\sigma^2$, and the asymmetry index $\beta$. These parameters were optimized during the fitting procedure, except for $N$ values, which were fixed according to the N2 structural model. In addition to the N2 model, alternative coordination geometries identified from the combined IR/Raman and DFT analysis, namely, NO, O2, NO2, and O4, were also evaluated. For each model, theoretical SS and MS contributions were generated starting from the corresponding DFT-optimized cluster geometry and treated following the same fitting protocol described above. Least-squares minimizations were carried out over the 3.2−10.7 $Å^{-1}$ $k$-range directly on the raw data, without preliminary background subtraction or Fourier filtering. In addition, nonstructural parameters were optimized, namely, the edge energy position $E_0$ and the energy positions and amplitudes of the double-electron excitations $KN_{2\&3}$, $KN_1$, and $KM_{4\&5}$. The amplitude reduction factor $S_0^2$ was constrained between 0.95 and 1.00.

## RESULTS AND DISCUSSION

### Raman Spectroscopy

Raman spectra of $AgTf_2N$ solutions in $[C_4mim][Tf_2N]$ at increasing metal concentrations were recorded to monitor the coordination of the $[Tf_2N]^-$ anion. As shown in Figure 1a, the

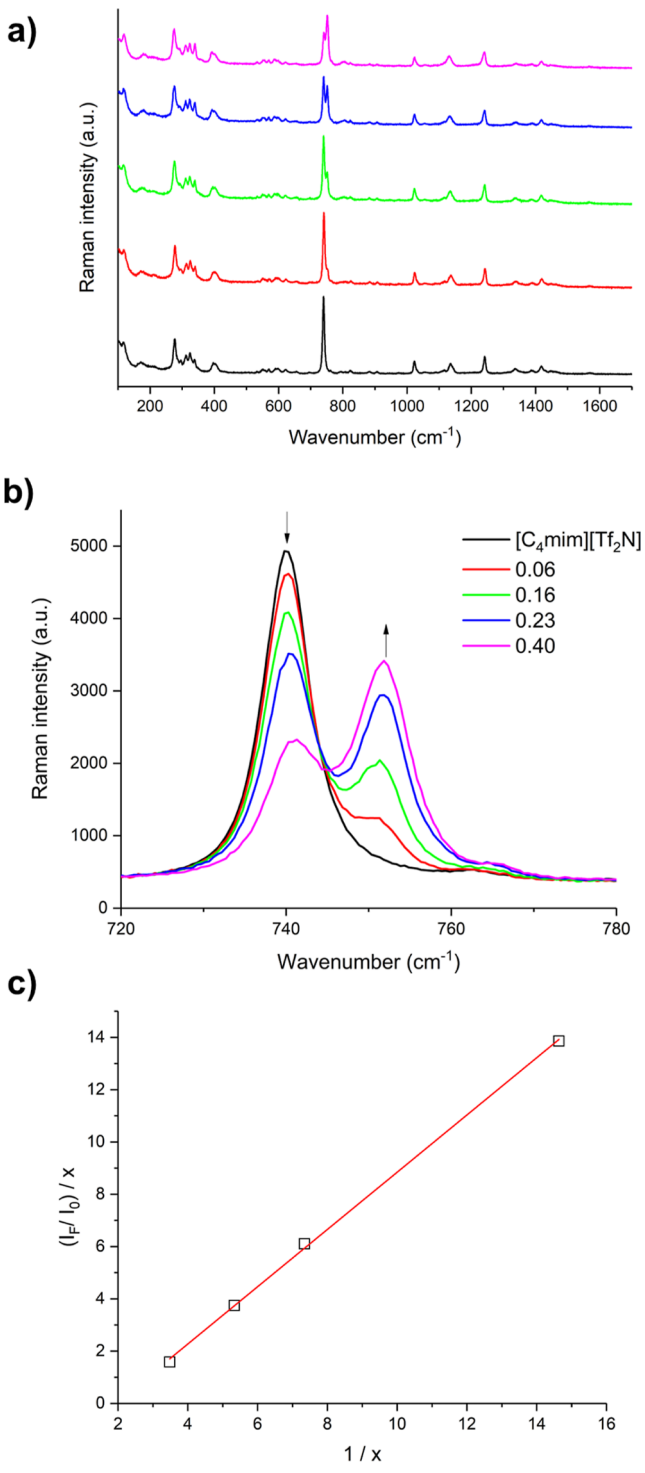


**Figure 1.** Raman spectra of $AgTf_2N$ solutions in $[C_4mim][Tf_2N]$ at an increasing (0.0−0.4) metal salt mole fraction ($x$) in the (a) 100−1700 $cm^{-1}$ and (b) 720−780 $cm^{-1}$ wavenumber ranges. (c) $(I_F/I_0)/x$ vs $1/x$ plot of deconvolved Raman bands in the 720−780 $cm^{-1}$ region. $R^2$ = 0.999.





https://doi.org/10.1021/acs.inorgchem.6c01404
Inorg. Chem. 2026, 65, 14023−14032

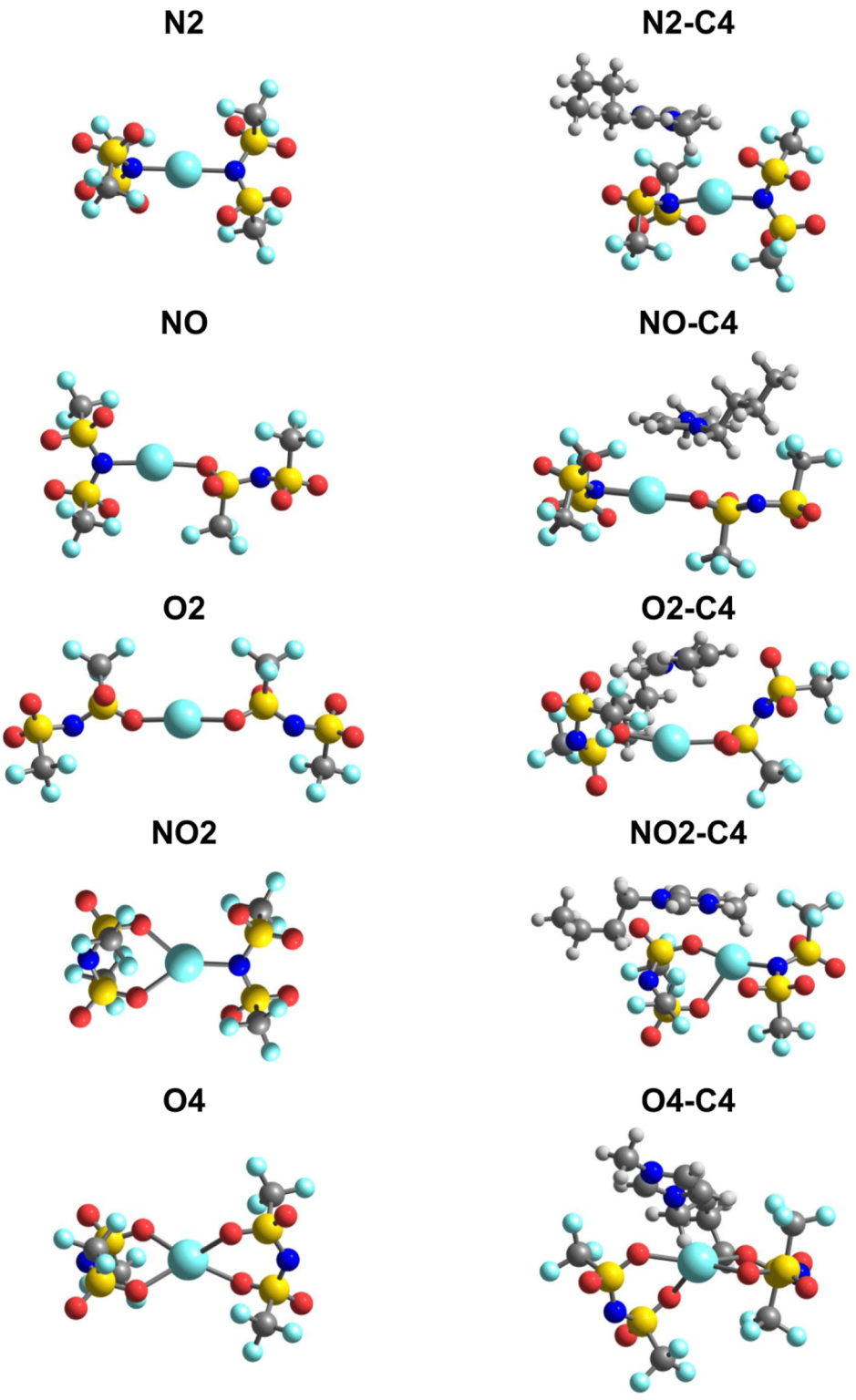


**Figure 2.** Minimum energy structures of the possible coordination isomers of $[Ag(Tf_2N)_2]^-$ (left) and of the $[C_4mim][Ag(Tf_2N)_2]$ ionic couples (right) at the $\omega$B97XD/def2-TZVP level in the SMD solvent.

most significant spectral changes upon metal salt addition occur in the 720−780 $cm^{-1}$ region. This spectral range contains a diagnostic vibrational feature for $[Tf_2N]^-$ coordination, arising from the overlap between the $-CF_3$ bending modes and the S−N−S stretching, commonly referred to as the $[Tf_2N]^-$ "breathing mode".[61,63,66] In neat $[C_4mim][Tf_2N]$, this band is centered at 740 $cm^{-1}$, and its intensity progressively decreases upon increasing the Ag mole fraction, while a new band appears at 752 $cm^{-1}$ (Figure 1b). The two bands evolve with respect to a well-defined isosbestic point, indicating an equilibrium between two dominant populations in solution, namely, free and coordinated $[Tf_2N]^-$.

The deconvolution of the overlapping contributions (Figure S2) allows separation of the bands associated with free and



https://doi.org/10.1021/acs.inorgchem.6c01404
Inorg. Chem. 2026, 65, 14023−14032

bound anions. This yields the plot in Figure 1c and, using eq 2, a value of $n = 1.92 \pm 0.15$ is determined. For comparison, the same data set was analyzed using the approach proposed by Lassègues et al.,[79] which assumes identical Raman scattering coefficients for the free and uncoordinated anion bands (Figure S3). This procedure provides a value of $n = 2.22 \pm 0.05$. Despite the different underlying assumptions, both methods consistently indicate that approximately two $[Tf_2N]^-$ anions are coordinated to $Ag^+$ in solution.

## FT-IR and DFT Results

To assess the coordination mode of the $[Tf_2N]^-$ anions toward $Ag^+$, DFT calculations were performed by exploring all plausible geometries of the $[Ag(Tf_2N)_2]^-$ complex. Five distinct coordination isomers were identified depending on the binding fashion of the anion. In the N2 structure, both $[Tf_2N]^-$ anions bind $Ag^+$ through the central nitrogen atoms. In the NO isomer, a mixed coordination is obtained, with one anion binding through nitrogen and the other through oxygen in a monodentate fashion. The O2 structure corresponds to bis *O*-monodentate coordination, whereas in the NO2 isomer, one anion coordinates via nitrogen, while the second adopts an *O*-bidentate mode. Finally, in the O4 structure, both anions bind in a bidentate fashion through oxygen atoms. In addition, it should be considered that the $[Tf_2N]^-$ anion is known to exist in two conformations, namely, a transoid (trans) and cisoid (cis), depending on the relative orientation of the—$CF_3$ groups with respect to the S−N−S plane.[67,80] Both cis and trans conformers of the $[Tf_2N]^-$ anion were optimized at the DFT level for the isolated anion and for the $[C_4mim][Tf_2N]$ ionic couple (Figure S4), evidencing a small energy difference (~0.3 kcal $mol^{-1}$ for the ionic couples), which is compatible with a conformational equilibrium shifted toward the trans form in the neat IL.[81] Since both rotamers can coordinate to a metal center, preliminary optimizations were performed for the N2 structure, considering both the cis,trans and cis,cis arrangements of the two coordinated anions (Figure S5), and their energy was compared to the trans,trans form (N2 in Figure 2). The trans,trans conformation was found to be the more stable one than the others (1.4 and 4.9 kcal $mol^{-1}$, respectively). Also, the FT-IR spectra in the 450−700 $cm^{-1}$ region of $[C_4mim][Tf_2N]$ solutions containing different amounts of Ag salt (Figure S6) display a small, but appreciable, change in intensity with a decrease of the peaks at 599 and 652 $cm^{-1}$ and an increase at 612 $cm^{-1}$, which have been previously[79] assigned to the cis (599 and 652 $cm^{-1}$) and trans (612 $cm^{-1}$) conformers of the $[Tf_2N]^-$ anion in the pure ILs. Thus, the relative intensity change suggests a shift of the conformational equilibrium toward the trans form induced by the coordination to the metal ion. Based on these results, and to limit the number of species to be considered for the DFT calculations, only the trans,trans arrangement for the coordinated anions was adopted for the coordination isomers considered in this work.

The minimum energy structures of the possible isomers for both the $[Ag(Tf_2N)_2]^-$ complexes and the $[C_4mim][Ag(Tf_2N)_2]$ ionic couples are shown in Figure 2, while the corresponding Ag−N and Ag−O bond distances are collected in Table S2. The relative stability of the isomers was evaluated in terms of free energy differences, defined as $\Delta G_{rel} = G_{isomer} - G_{N2}$ (or $G_{N2-C4}$ for the ionic couples), where the N2 (or N2−C4) structure is taken as the reference. The resulting values are reported in Table 1 for both gas phase and continuum solvent conditions. For the $[Ag(Tf_2N)_2]^-$ complexes in solvent, the stability order is N2 > NO2 > O4 ~ NO > O2. A similar trend is obtained for the $[C_4mim][Ag(Tf_2N)_2]$ ionic couples, with the order N2−C4 > NO2−C4 ~ NO−C4 > O4−C4 > O2−C4. In both series, the N2 (and N2−C4) isomer is predicted to be the most stable in both gas phase and in continuum solvent, with an energy difference of 3.4 kcal $mol^{-1}$ (N2) and 3.8 kcal $mol^{-1}$ (N2−C4) relative to the next most stable species in solvent (NO2/NO2−C4, Table 1). Such non-negligible energy gaps suggest the possible predominance of the N2 coordination motif in solution.

**Table 1. Relative Free Energies ($\Delta G_{rel}$, kcal $mol^{-1}$) of the $[Ag(Tf_2N)_2]^-$ Isomers and the $[C_4mim][Ag(Tf_2N)_2]$ Ionic Couples in the Gas Phase and in SMD Solvent**

| isomer | gas | solv | isomer | gas | solv |
|---|---|---|---|---|---|
| N2 | 0.0 | 0.0 | N2−C4 | 0.0 | 0.0 |
| NO | 6.8 | 6.1 | NO−C4 | 2.2 | 5.3 |
| O2 | 13.7 | 11.2 | O2−C4 | 7.1 | 9.8 |
| NO2 | 1.2 | 3.4 | NO2−C4 | 3.2 | 3.8 |
| O4 | 3.5 | 5.4 | O4−C4 | 0.7 | 5.7 |

The experimental FT-IR spectra in the 950−1450 $cm^{-1}$ region (Figure 3) show clear and systematic changes upon increasing the Ag molar fraction. In particular, when $AgTf_2N$ is dissolved, the intense band at 1051 $cm^{-1}$ present in the neat IL (black spectrum in Figure 3) decreases in intensity and, simultaneously, a new feature appears at 1004 $cm^{-1}$. At the same time, the absorbance at 1132 $cm^{-1}$ slightly increases.

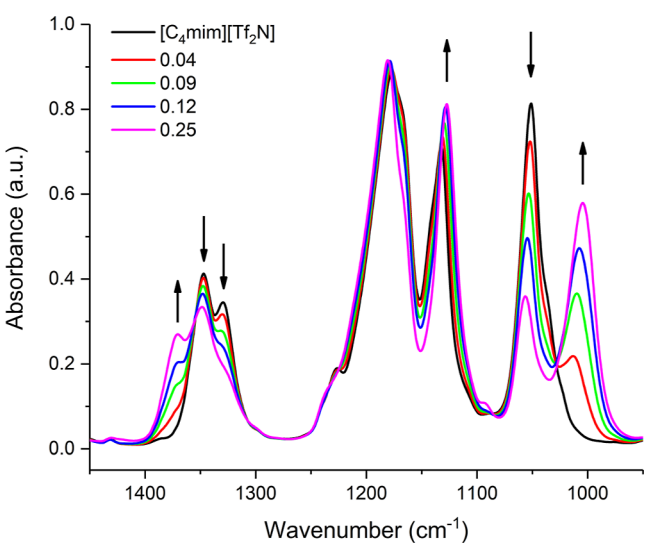


**Figure 3.** Experimental FT-IR spectra of $AgTf_2N$ solutions in $[C_4mim][Tf_2N]$ at increasing $x$ (0.0−0.25). Black arrows indicate the direction of peak changes upon addition of $AgTf_2N$.

The vibrational analysis of the minimum-energy structure of the $[C_4mim][Tf_2N]$ ionic couple (black spectrum in Figure 4) predicts two intense bands at 1078 and 1200 $cm^{-1}$ (the latter composed by two components at 1200 and 1173 $cm^{-1}$), associated with asymmetric S−N−S stretching modes (Table S1). The calculated frequencies are in agreement with the experimental bands at 1051 and 1132 $cm^{-1}$ (Figure 3), which were also previously assigned to S−N−S vibrations.[63] The calculated IR spectra (Figure 4) for the $[C_4mim][Ag(Tf_2N)_2]$ complexes in Figure 2 differ markedly from that of the




https://doi.org/10.1021/acs.inorgchem.6c01404
Inorg. Chem. 2026, 65, 14023−14032

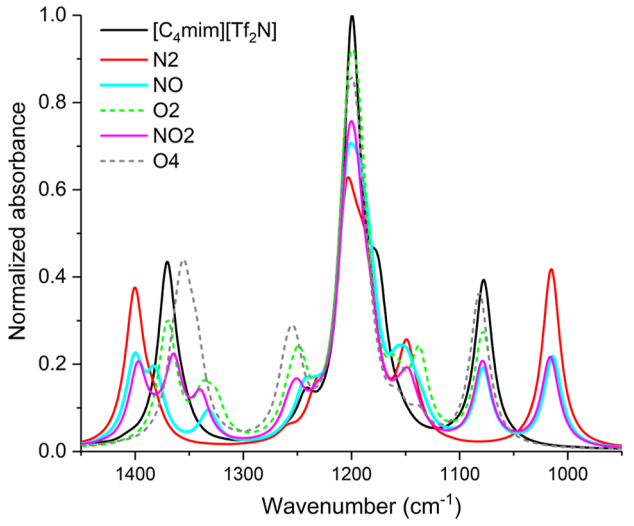


**Figure 4.** Calculated FT-IR spectra in the 950−1450 $cm^{-1}$ range for $[C_4mim][Tf_2N]$ and for the $[C_4mim][Ag(Tf_2N)_2]$ complexes, computed at the ωB97XD/def2-TZVP level in the SMD solvent. Vibrational wavenumbers were scaled by a factor of 0.9914[82] and spectral bands were generated using Gaussian functions with a 10 $cm^{-1}$ half-width at half-maximum.

$[C_4mim][Tf_2N]$ ionic couple, consistent with the experimental changes observed upon addition of the metal salt to the neat IL (Figure 3). Notably, the isomers in which the $[Tf_2N]^-$ anion coordinates via the nitrogen atom (N2−C4, NO−C4, and NO2−C4) display a new S−N−S stretching band at lower wavenumbers with respect to that calculated for the $[C_4mim][Tf_2N]$ ionic couple (Figure 4 and Table S1). The calculated maxima centered at 1015 $cm^{-1}$ for N2−C4, NO−C4, and NO2−C4 are in good agreement with the new experimental band appearing at 1004 $cm^{-1}$ upon metal salt dissolution. Importantly, this feature is absent for the isomers where coordination occurs exclusively through oxygen atoms (O2−C4 and O4−C4, dashed spectra in Figure 4). This downshift of the S−N−S stretching frequency therefore emerges as a spectral fingerprint of *N*-coordination of the $[Tf_2N]^-$ anion. Moreover, the calculated spectra of the *O*-coordinated species predict intense bands at 1082 $cm^{-1}$ (O4−C4) and 1078 $cm^{-1}$ (O2−C4), which are not detected experimentally. The N2−C4 structure is the only isomer that does not present spectral features in this region. Altogether with the relative stabilities in Table 1, these observations suggest that O-coordinated species are unlikely to be present in significant amounts.

Additional evidence arises from the 1300−1400 $cm^{-1}$ region. In the experimental spectrum of the neat IL, a band with two maxima at 1347 and 1330 $cm^{-1}$ decreases in intensity upon addition of the metal salt, while a new band appears at 1371 $cm^{-1}$ (Figure 3). The calculated spectrum of $[C_4mim][Tf_2N]$ presents a single band centered at 1370 $cm^{-1}$, resulting from the combination of two vibrational modes at 1370 and 1355 $cm^{-1}$, assigned to S═O stretching motions (Figure 4 and Table S2). In the calculated spectra of the N2−C4 isomer, this band shifts to higher wavenumbers, with a calculated maximum at 1400 $cm^{-1}$. Similarly, NO−C4 and NO2−C4 display weaker and shifted bands at 1400 and 1398 $cm^{-1}$, respectively. In contrast, the spectrum of O2−C4 exhibits a new band centered at 1335 $cm^{-1}$, corresponding to the stretching of uncoordinated S═O groups. In the case of O4−C4, this feature is located at 1356 $cm^{-1}$ with a shoulder at 1343 $cm^{-1}$. The overall results show that only *N*-coordinated species produce a new band at higher wavenumbers relative to $[C_4mim][Tf_2N]$, in agreement with the experimental spectra showing a new band at 1371 $cm^{-1}$ upon dissolution of the silver salt (Figure 3). Furthermore, no new bands appear below 1330 $cm^{-1}$ in the experimental spectra, whereas such features are predicted for *O*-coordinated structures (dashed spectra in Figure 4).

Overall, the comparison between experimental and calculated FT-IR spectra (Figures 3 and 4), together with the computed relative free energies (Table 1), consistently supports that the $Ag^+$ ion predominantly adopts a linear coordination with two $[Tf_2N]^-$ anions bound through the central nitrogen atom, with *O*-bound species being disfavored.

## XAS Results

The EXAFS analysis of the 0.1 mol $L^{-1}$ $AgTf_2N$ solution in $[C_4mim][Tf_2N]$ was performed to obtain a structural description of the local coordination environment of the $Ag^+$ ion. The N2 structural model was tested to confirm the presence and predominance of this species in solution. The best-fit results are shown in Figure 5. In the upper panel, the Ag−N, Ag−S, and Ag−O SS theoretical signals, as well as the Ag−N−S and N−Ag−N MS ones, are reported together with their sum into the total theoretical contribution, which is compared to the experimental data and the resulting residuals. A good agreement between the calculated and the experimental spectra is observed, as further confirmed by the corresponding Fourier transforms (FTs) reported in the lower panel of Figure 5, calculated over the 3.2−10.0 $Å^{-1}$ *k*-range. The optimized $E_0$ value was found to be 2.7 eV above the first inflection point of the experimental spectrum, while $S_0^2$ was 0.97.

The structural parameters determined for the two-body distributions are listed in Table 2, while the refined values for the Ag−N−S and N−Ag−N bond angles resulted in 118(6)° and 179(5)°, respectively. The first-shell contribution is dominated by the Ag−N signal, with an average distance of 2.23(2) Å, corresponding to the main peak in the FT. This value is in good agreement with the Ag−N distance obtained from the DFT-optimized structure (2.209 Å, Table S2), within the experimental uncertainty. The Ag−S signal is also marked in amplitude, reflecting the strong backscattering contribution of sulfur atoms located at an average distance of 3.31(3) Å, and dominates the second FT peak centered at about 3 Å. In contrast, the MS contributions and the Ag−O signal from the more distant oxygen atoms at 3.35(4) Å are weaker in intensity. The relatively small $\sigma^2$ value for the Ag−N distribution indicates a well-defined first coordination shell, whereas the larger $\sigma^2$ values associated with Ag−S and Ag−O reflect increased structural disorder at longer distances, consistent with the intrinsic flexibility of a structurally complex anion such as $[Tf_2N]^-$.[17,18,49,57] However, this interpretation must take into account the well-known correlation between path degeneracies and Debye−Waller factors in the EXAFS region and the uncertainty that arises in the determination of these parameters. Overall, the refined bond distances and angles are consistent with the N2 geometry, and the EXAFS analysis is therefore compatible with this coordination motif of the $Ag^+$ ion in the IL solution.

To evaluate alternative possible geometries, additional EXAFS fits were also performed for the NO, O2, NO2, and O4 models. The results are shown in Figure S7, where the total theoretical EXAFS signals for each geometry are compared




https://doi.org/10.1021/acs.inorgchem.6c01404
Inorg. Chem. 2026, 65, 14023−14032

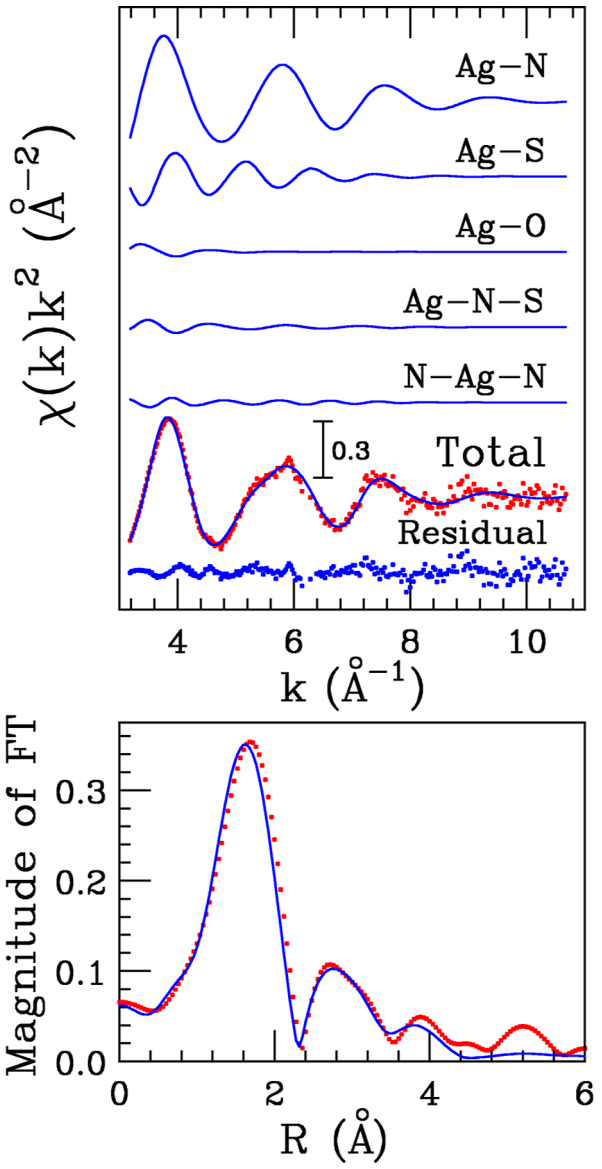


**Figure 5.** Upper panel: Ag K-edge EXAFS analysis of the 0.1 mol $L^{-1}$ $AgTf_2N$ solution in $[C_4mim][Tf_2N]$. From top to bottom: Ag−N, Ag−S, and Ag−O SS theoretical signals, Ag−N−S and N−Ag−N MS theoretical signals, and total theoretical spectrum (blue lines) compared with the experimental one (red dots) and resulting residuals (blue dots). Lower panel: nonphase-shift-corrected FTs of the total theoretical signal (blue line) and of the experimental data (red dots).

**Table 2. Best-Fit Structural Parameters for the Ag−N, Ag−S, and Ag−O Two-Body Distributions Obtained from the Ag K-Edge EXAFS Analysis of the 0.1 mol $L^{-1}$ $AgTf_2N$ Solution in $[C_4mim][Tf_2N]$. *N* Is the Path Degeneracy, *R* the Average Distance, $\sigma^2$ the Debye−Waller Factor, and $\beta$ the Asymmetry Index**

| | *N* | *R* (Å) | $\sigma^2$ (Å$^{-2}$) | $\beta$ |
|---|---|---|---|---|
| Ag−N | 2.0 | 2.23(2) | 0.009(2) | 0.0(1) |
| Ag−S | 4.0 | 3.31(3) | 0.033(4) | 0.0(2) |
| Ag−O | 4.0 | 3.35(4) | 0.082(5) | 0.0(3) |

with the experimental data (Figure S7a), together with the corresponding FTs (Figure S7b). Alternative models generally show progressively poorer agreement with both the experimental EXAFS signal and FT, while the comparison with the fit obtained for the N2 model (Figure 5) indicates that the N2 structure provides the best agreement with the experimental data. The NO model yields a partially satisfactory description, consistent with its retention of one Ag−N interaction, whereas *O*-dominated and higher-coordination models progressively worsen the agreement. In particular, the models with first-shell CNs greater than two, such as NO2 and O4, tend to overestimate the EXAFS amplitude and the intensity of the first FT peak. The overall results indicate that, although minor contributions from alternative structural motifs cannot be completely ruled out, particularly mixed O/N coordinations like NO or NO2, the EXAFS analysis supports N2 as the dominant species under the investigated conditions. Taken together, these findings point to a specific coordination behavior of the $Ag^+$ ion in solution that differs markedly from that observed for other divalent transition metals[17−20,57−62] and also for monovalent ions such as $Li^+$ or $Na^+$,[67,83] which present the anion coordinated exclusively via oxygen in monodentate or chelating modes. This behavior is in agreement with the HSAB theory, which predicts a preferential interaction of the soft acid $Ag^+$ with the soft base imide nitrogen atom[51] and has previously been identified in the solid state also for other soft metal ions ($Cu^+$ and $Au^+$).[84,85]

## CONCLUSIONS

In this work, the solvation structure of the $Ag^+$ ion in the $[C_4mim][Tf_2N]$ IL has been elucidated through the combination of Raman and FT-IR spectroscopy, DFT calculations, and XAS. Raman measurements in the 720−780 $cm^{-1}$ region reveal the progressive conversion of free to coordinated $[Tf_2N]^-$ anions upon addition of $AgTf_2N$. Quantitative analysis of the Raman bands indicates that, over the investigated concentration range, each $Ag^+$ ion is coordinated by two $[Tf_2N]^-$ anions.

DFT calculations allowed the discrimination among possible $[Ag(Tf_2N)_2]^-$ coordination isomers. The computed relative free energies and vibrational signatures, in direct comparison with the evolution of the experimental FT-IR spectra, consistently identify a predominant complex in which $Ag^+$ is linearly coordinated by two monodentate $[Tf_2N]^-$ ligands through the central nitrogen atom. In contrast, *O*-bound coordination modes are both energetically disfavored and spectroscopically inconsistent with the experimental observations, suggesting that their contribution, if present, is minor.

The EXAFS analysis provides a structural validation of this model, revealing a well-defined first coordination shell characterized by two Ag−N interactions at 2.23(2) Å and an almost collinear N−Ag−N arrangement. Although the presence of minor species in equilibrium cannot be completely ruled out, the combined experimental and theoretical evidence clearly identifies the linear *N*-bound motif as the dominant solvation structure of $Ag^+$ in $[C_4mim][Tf_2N]$.

To the best of our knowledge, these results provide the first unambiguous structural evidence of linearly coordinated $Ag^+$ in an ionic liquid. The marked contrast with the coordination structures previously observed in molecular solvents and in other ILs highlights the strong sensitivity of $Ag^+$ speciation to the solvation environment and underscores the critical role of the anion in dictating the metal ion solvation structure.




https://doi.org/10.1021/acs.inorgchem.6c01404
Inorg. Chem. 2026, 65, 14023−14032

## ■ ASSOCIATED CONTENT

### Supporting Information

The Supporting Information is available free of charge at https://pubs.acs.org/doi/10.1021/acs.inorgchem.6c01404.

Schematic representation of EXAFS single and multiple scattering paths; Raman band deconvolution and analysis of the 720−780 $cm^{-1}$ region; optimized geometries of the conformers of the $[Tf_2N]^-$ anion and $[C_4mim][Tf_2N]$ ionic couple and the $[Ag(Tf_2N)_2]^-$ complexes; 450−700 $cm^{-1}$ region of the experimental FT-IR spectra; EXAFS analysis using alternative coordination models; calculated vibrational frequencies and intensities for ionic species and complexes; calculated Ag−N and Ag−O bond lengths for optimized structures; and Cartesian coordinates of the obtained minimum energy structures (PDF)

## ■ AUTHOR INFORMATION


### Corresponding Author

**Andrea Melchior** − *Università degli Studi di Udine, Dipartimento Politecnico di Ingegneria e Architettura, Udine 33100, Italy;* orcid.org/0000-0002-5265-1396; Email: andrea.melchior@uniud.it

### Authors

**Matteo Busato** − *Sapienza Università di Roma, Dipartimento di Chimica, Roma 00185, Italy;* orcid.org/0000-0002-9450-0481

**Martina Sanadar** − *Centre de Biophysique Moléculaire, CNRS UPR 4301, Université d'Orléans, Orléans 45071, France*

**Paola D'Angelo** − *Sapienza Università di Roma, Dipartimento di Chimica, Roma 00185, Italy;* orcid.org/0000-0001-5015-8410

Complete contact information is available at: https://pubs.acs.org/10.1021/acs.inorgchem.6c01404


### Notes

The authors declare no competing financial interest.

## ■ ACKNOWLEDGMENTS

The authors thank Elettra Sincrotrone Trieste S.C.p.A. and its staff for providing synchrotron radiation beam time and laboratory facilities (proposal n. 20190065). A.M. thanks M. Danielis for the experimental support. This work was supported by the University of Udine in the framework of the Strategic Plan 2022-25—Interdepartmental Research Project ESPeRT.

## ■ REFERENCES


(1) Kaur, G.; Kumar, H.; Singla, M. Diverse applications of ionic liquids: A comprehensive review. *J. Mol. Liq.* **2022**, *351*, 118556.

(2) Yang, Y.; Walton, A.; Sheridan, R.; Güth, K.; Gauß, R.; Gutfleisch, O.; Buchert, M.; Steenari, B.-M.; Van Gerven, T.; Jones, P. T.; Binnemans, K. REE Recovery from End-of-Life NdFeB Permanent Magnet Scrap: A Critical Review. *J. Sustain. Metall.* **2017**, *3*, 122−149.

(3) Kovačević, A.; Tolazzi, M.; Sanadar, M.; Melchior, A. Hydrometallurgical recovery of metals from spent lithium-ion batteries with ionic liquids and deep eutectic solvents. *J. Environ. Chem. Eng.* **2024**, *12*, 113248.

(4) Kovačević, A.; Ricardo García, J. A.; Tolazzi, M.; Melchior, A.; Sanadar, M. Selective Co(II) and Ni(II) Separation Using the Trihexyl(tetradecyl)phosphonium Decanoate Ionic Liquid. *Molecules* **2024**, *29*, 4545.

(5) Khalid, H. M.; Santos, R. M. Deep eutectic solvents and ionic liquids in hydrometallurgical recovery of metals - A review of recent advances and challenges. *Hydrometallurgy* **2025**, *238*, 106571.

(6) Zhang, X.; Wang, Z.; Li, Z. Research progress of ionic liquids in recycling waste lithium-ion batteries: from metal extraction to material regeneration. *Sep. Purif. Technol.* **2025**, *379*, 134850.

(7) Armand, M.; Endres, F.; MacFarlane, D.; Ohno, H.; Scrosati, B. Ionic-liquid Materials for the Electrochemical Challenges of the Future. *Nat. Mater.* **2009**, *8*, 621−629.

(8) MacFarlane, D. R.; Tachikawa, N.; Forsyth, M.; Pringle, J. M.; Howlett, P. C.; Elliott, G. D.; Davis, J. H.; Watanabe, M.; Simon, P.; Angell, C. A. Energy applications of ionic liquids. *Energy Environ. Sci.* **2014**, *7*, 232−250.

(9) Kaur, H.; Thakur, A.; Thakur, R. C.; Kumar, A. A Review on Multifaceted Role of Ionic Liquids in Modern Energy Storage Systems: From Electrochemical Performance to Environmental Sustainability. *Energy Fuels* **2025**, *39*, 3703−3734.

(10) Makhlooghiazad, F.; Huang, L.; Byrne, N.; Howlett, P. C.; Forsyth, M. Ionic Liquids Electrolytes for High Performance Sodium Batteries Chemistry, Composition, and Interfaces. *Adv. Energy Mater.* **2026**, No. e06236.

(11) Zhang, Q.; Wang, Q.; Zhang, S.; Lu, X.; Zhang, X. Electrodeposition in Ionic Liquids. *ChemPhysChem* **2016**, *17*, 335−351.

(12) Costa, J. G. d. R. d.; Costa, J. M.; Almeida Neto, A. F. d. Progress on Electrodeposition of Metals and Alloys Using Ionic Liquids as Electrolytes. *Metals* **2022**, *12*, 2095.

(13) Nahian, M. K.; Reddy, R. G. Green Electrodeposition of Common Lanthanide Rare Earth Metals Using Ionic Liquids: Challenges and Opportunities. *J. Electrochem. Soc.* **2025**, *172*, 022503.

(14) Sood, K.; Saini, Y.; Thakur, K. K. Ionic liquids in catalysis: A review. *Mater. Today: Proc.* **2023**, *81*, 739−744.

(15) Dupont, J.; Leal, B. C.; Lozano, P.; Monteiro, A. L.; Migowski, P.; Scholten, J. D. Ionic Liquids in Metal, Photo-, Electro-, and (Bio) Catalysis. *Chem. Rev.* **2024**, *124*, 5227−5420.

(16) Mandai, T.; Yoshida, K.; Ueno, K.; Dokko, K.; Watanabe, M. Criteria for solvate ionic liquids. *Phys. Chem. Chem. Phys.* **2014**, *16*, 8761−8772.

(17) Busato, M.; D'Angelo, P.; Melchior, A. Solvation of $Zn^{2+}$ ion in 1-alkyl-3-methylimidazolium bis(trifluoromethylsulfonyl)imide ionic liquids: a molecular dynamics and X-ray absorption study. *Phys. Chem. Chem. Phys.* **2019**, *21*, 6958−6969.

(18) Busato, M.; D'Angelo, P.; Lapi, A.; Tolazzi, M.; Melchior, A. Solvation of $Co^{2+}$ ion in 1-butyl-3-methylimidazolium bis-(trifluoromethylsulfonyl)imide ionic liquid: A molecular dynamics and X-ray absorption study. *J. Mol. Liq.* **2020**, *299*, 112120.

(19) Busato, M.; Lapi, A.; D'Angelo, P.; Melchior, A. Coordination of the $Co^{2+}$ and $Ni^{2+}$ ions in $Tf_2N^-$ based Ionic Liquids: A Combined X-ray Absorption and Molecular Dynamics Study. *J. Phys. Chem. B* **2021**, *125*, 6639−6648.

(20) Melchior, A.; Gaillard, C.; Gràcia Lanas, S.; Tolazzi, M.; Billard, I.; Georg, S.; Sarrasin, L.; Boltoeva, M. Nickel(II) Complexation with Nitrate in Dry $[C_4mim][Tf_2N]$ Ionic Liquid: A Spectroscopic, Microcalorimetric, and Molecular Dynamics Study. *Inorg. Chem.* **2016**, *55*, 3498−3507.

(21) Hartley, J. M.; Ip, C.-M.; Forrest, G. C. H.; Singh, K.; Gurman, S. J.; Ryder, K. S.; Abbott, A. P.; Frisch, G. EXAFS study into the speciation of metal salts dissolved in ionic liquids and deep eutectic solvents. *Inorg. Chem.* **2014**, *53*, 6280−6288.

(22) Takemura, S.; Kawakami, S.; Harada, M.; Iida, M. Solvation structure of a copper(II) ion in protic ionic liquids comprising N-hexylethylenediamine. *Inorg. Chem.* **2014**, *53*, 9667−9678.

(23) Busato, M.; D'Angelo, P.; Lapi, A.; Tavani, F.; Veclani, D.; Tolazzi, M.; Melchior, A. Unraveling the $Ag^+$ ion coordination and solvation thermodynamics in the 1-butyl-3-methylimidazolium tetrafluoroborate ionic liquid. *J. Mol. Liq.* **2023**, *387*, 122654.

(24) Sun, P.-P.; Song, H.-I.; Kim, T.-Y.; Min, B.-J.; Cho, S.-Y. Recovery of Silver from the Nitrate Leaching Solution of the Spent Ag/$\alpha$-$Al_2O_3$ Catalyst by Solvent Extraction. *Ind. Eng. Chem. Res.* **2014**, *53*, 20241−20246.
(25) Laki, S.; Arabi Shamsabadi, A.; Seidi, F.; Soroush, M. Sustainable Recovery of Silver from Deactivated Catalysts Using a Novel Process Combining Leaching and Emulsion Liquid Membrane Techniques. *Ind. Eng. Chem. Res.* **2018**, *57*, 13821−13832.
(26) Domańska, U.; Rękawek, A. Extraction of metal ions from aqueous solutions using imidazolium based ionic liquids. *J. Solution Chem.* **2009**, *38*, 739−751.
(27) Shimojo, K.; Goto, M. Solvent extraction and stripping of silver ions in room-temperature ionic liquids containing calixarenes. *Anal. Chem.* **2004**, *76*, 5039−5044.
(28) Wei, G.-T.; Yang, Z.; Chen, C.-J. Room temperature ionic liquid as a novel medium for liquid/liquid extraction of metal ions. *Anal. Chim. Acta* **2003**, *488*, 183−192.
(29) Basile, A.; Bhatt, A. I.; O'Mullane, A. P.; Bhargava, S. K. An investigation of silver electrodeposition from ionic liquids: Influence of atmospheric water uptake on the silver electrodeposition mechanism and film morphology. *Electrochim. Acta* **2011**, *56*, 2895−2905.
(30) Schaltin, S.; Brooks, N. R.; Stappers, L.; Van Hecke, K.; Van Meervelt, L.; Binnemans, K.; Fransaer, J. High current density electrodeposition from silver complex ionic liquids. *Phys. Chem. Chem. Phys.* **2012**, *14*, 1706−1715.
(31) Depuydt, D.; Brooks, N. R.; Schaltin, S.; VanMeervelt, L.; Fransaer, J.; Binnemans, K. Silver-Containing Ionic Liquids with Alkylamine Ligands. *ChemPlusChem* **2013**, *78*, 578−588.
(32) Ren, T.; Patel, M.; Blok, K. Olefins from conventional and heavy feedstocks: Energy use in steam cracking and alternative processes. *Energy* **2006**, *31*, 425−451.
(33) Sanchez, C. M.; Song, T.; Brennecke, J. F.; Freeman, B. D. Hydrogen Stable Supported Ionic Liquid Membranes with Silver Carriers: Propylene and Propane Permeability and Solubility. *Ind. Eng. Chem. Res.* **2020**, *59*, 5362−5370.
(34) Park, S.; Morales-Collazo, O.; Freeman, B.; Brennecke, J. F. Ionic Liquid Stabilizes Olefin Facilitated Transport Membranes Against Reduction. *Angew. Chem., Int. Ed.* **2022**, *61*, No. e202202895.
(35) Wu, X.; Li, X.; Xu, L.; He, W.; Zhou, Z.; Liu, W.; Zhang, F.; Ren, Z. Application of silver ionic liquid in the separation of olefin and alkane. *J. Chem. Technol. Biotechnol.* **2022**, *97*, 1207−1214.
(36) Wu, Q.; Li, G.; Cheng, Y.; Fan, B.; Bai, Y.; Zhang, N.; Wang, Z.; Zhang, X.; Zhang, S. Efficient separation of ethylene/ethane by incorporation of silver salts into protic imidazole ionic liquids. *Chem. Eng. J.* **2023**, *461*, 141942.
(37) Persson, I.; Nilsson, K. B. Coordination Chemistry of the Solvated Silver(I) Ion in the Oxygen Donor Solvents Water, Dimethyl Sulfoxide, and N,N'-Dimethylpropyleneurea. *Inorg. Chem.* **2006**, *45*, 7428−7434.
(38) Tsutsui, Y.; Sugimoto, K.-i.; Wasada, H.; Inada, Y.; Funahashi, S. EXAFS and ab Initio Molecular Orbital Studies on the Structure of Solvated Silver(I) Ions. *J. Phys. Chem. A* **1997**, *101*, 2900−2905.
(39) Prasetyo, N.; Hidayat, Y. Lability of the first solvation shell of silver cations in liquid ammonia: A quantum mechanical charge field molecular dynamics simulation study. *J. Mol. Liq.* **2022**, *350*, 118517.
(40) Tofoni, A.; Busato, M.; Colella, A.; Melchior, A.; D'Angelo, P. In-Depth XANES and EXAFS Characterization of the $Ag^+$ Ion Coordination in Dimethyl Sulfoxide Solution. *J. Phys. Chem. B* **2024**, *128*, 8065−8073.
(41) Zanonato, P. L.; Di Bernardo, P.; Melchior, A.; Tolazzi, M.; Polese, P.; Busato, M. Solvent and structural effects on Silver(I) complex formation: thermodynamics and modeling. *J. Therm. Anal. Calorim.* **2022**, *147*, 5501−5509.
(42) Luigi Zanonato, P.; Di Bernardo, P.; Melchior, A.; Busato, M.; Tolazzi, M. Lanthanides(III) and silver(I) complex formation with triamines in DMSO: the effect of ligand cyclization. *Inorg. Chim. Acta* **2020**, *503*, 119392.
(43) Zanonato, P. L.; Melchior, A.; Busato, M.; Di Bernardo, P.; Tolazzi, M. Silver(I) complexes with long-chain diamines in non-aqueous solvents. *J. Therm. Anal. Calorim.* **2019**, *138*, 3257−3265.
(44) Melchior, A.; Tolazzi, M.; Polese, P.; Zanonato, P. L. Thermodynamics of complex formation of silver(I) with N-donor ligands in non-aqueous solvents. *J. Therm. Anal. Calorim.* **2017**, *130*, 461−469.
(45) Melchior, A.; Peralta, E.; Valiente, M.; Tavagnacco, C.; Endrizzi, F.; Tolazzi, M. Interaction of $d^{10}$ metal ions with thioether ligands: a thermodynamic and theoretical study. *Dalton Trans.* **2013**, *42*, 6074−6082.
(46) Del Piero, S.; Fedele, R.; Melchior, A.; Portanova, R.; Tolazzi, M.; Zangrando, E. Solvation effects on the stability of silver(I) complexes with pyridine-containing ligands studied by thermodynamic and DFT methods. *Inorg. Chem.* **2007**, *46*, 4683−4691.
(47) Melchior, A.; Sanadar, M.; Cappai, R.; Tolazzi, M. Entropy and enthalpy effects on metal complex formation in non-aqueous solvents: the case of silver(I) and monoamines. *Entropy* **2022**, *24*, 1253.
(48) Pliego, J. R. Car-Parrinello molecular dynamics study of CuF,AgF,$CuPF_6$and$AgPF_6$ in acetonitrile solvent and Cluster-Continuum calculation of the solvation free energy of Cu(I),Ag(I)-andLi(I). *J. Mol. Liq.* **2022**, *359*, 119368.
(49) Busato, M.; Melchior, A.; Migliorati, V.; Colella, A.; Persson, I.; Mancini, G.; Veclani, D.; D'Angelo, P. Elusive Coordination of the $Ag^+$ Ion in Aqueous Solution: Evidence for a Linear Structure. *Inorg. Chem.* **2020**, *59*, 17291−17302.
(50) Cotton, F. A.; Wilkinson, G. *Advanced Inorganic Chemistry*, 4th ed.; John Wiley & Sons, 1980.
(51) Di Bernardo, P.; Melchior, A.; Portanova, R.; Tolazzi, M.; Zanonato, P. L. Complex formation of N-donor ligands with group 11 monovalent ions. *Coord. Chem. Rev.* **2008**, *252*, 1270−1285.
(52) Nilsson, K. B.; Persson, I.; Kessler, V. G. Coordination Chemistry of the Solvated $Ag^I$ and $Au^I$ Ions in Liquid and Aqueous Ammonia, Trialkyl and Triphenyl Phosphite, and Tri-n-butylphosphine Solutions. *Inorg. Chem.* **2006**, *45*, 6912−6921.
(53) Pham, T. A.; Horwood, C.; Maiti, A.; Peters, V.; Bunn, T.; Stadermann, M. Solvation Properties of Silver and Copper Ions in a Room Temperature Ionic Liquid: A First-Principles Study. *J. Phys. Chem. B* **2018**, *122*, 12139−12146.
(54) Imai, M.; Tanabe, I.; Ozaki, Y.; Fukui, K. Solvation properties of silver ions in ionic liquids using attenuated total reflectance ultraviolet spectroscopy. *J. Mol. Liq.* **2022**, *364*, 119998.
(55) Regel-Rosocka, M.; Materna, K. In *Ionic Liquids in Separation Technology*; Pérez De Los Ríos, A., Hernández Fernández, F. J., Eds.; Elsevier: Amsterdam, 2014; pp 153−188.
(56) Makanyire, T.; Sanchez-Segado, S.; Jha, A. Separation and recovery of critical metal ions using ionic liquids. *Adv. Manuf.* **2016**, *4*, 33−46.
(57) Sessa, F.; Migliorati, V.; Serva, A.; Lapi, A.; Aquilanti, G.; Mancini, G.; D'Angelo, P. On the Coordination of $Zn^{2+}$ Ion in $Tf_2N^-$ Based Ionic Liquids: Structural and Dynamic Properties Depending on the Nature of the Organic Cation. *Phys. Chem. Chem. Phys.* **2018**, *20*, 2662−2675.
(58) Fujii, K.; Nonaka, T.; Akimoto, Y.; Umebayashi, Y.; Ishiguro, S.-I. Solvation Structures of Some Transition Metal(II) Ions in a Room-Temperature Ionic Liquid, 1-Ethyl-3-methylimidazolium Bis-(trifluoromethanesulfonyl)amide. *Anal. Sci.* **2008**, *24*, 1377−1380.
(59) Matsumiya, M.; Kamo, Y.; Hata, K.; Tsunashima, K. Solvation structure of iron group metal ion in TFSA-based ionic liquids investigated by Raman spectroscopy and DFT calculations. *J. Mol. Struct.* **2013**, *1048*, 59−63.
(60) Bortolini, O.; Chiappe, C.; Ghilardi, T.; Massi, A.; Pomelli, C. S. Dissolution of Metal Salts in Bis(trifluoromethylsulfonyl)imide-Based Ionic Liquids: Studying the Affinity of Metal Cations Toward a "Weakly Coordinating" Anion. *J. Phys. Chem. A* **2015**, *119*, 5078−5087.
(61) Tsuchida, Y.; Matsumiya, M.; Tsunashima, K. Solvation structure for Fe(II), Co(II) and Ni(II) complexes in $[P_{2225}][NTf_2]$

ionic liquids investigated by Raman spectroscopy and DFT calculation. *J. Mol. Liq.* **2018**, *269*, 8−13.
(62) Maseda, M.; Takamuku, T. $^{1}$H, $^{13}$C, $^{15}$N NMR, and DFT Studies on Complex Formation of Zinc(II) Ion with Ethylenediamine in Ionic Liquid [$C_2$mIm][TFSA]. *J. Phys. Chem. B* **2024**, *128*, 9500−9511.
(63) Liu, T.; Danten, Y.; Grondin, J.; Vilar, R. Solvation of AgTFSI in 1-ethyl-3-methylimidazolium bis(trifluoromethylsulfonyl)imide ionic liquid investigated by vibrational spectroscopy and DFT calculations. *J. Raman Spectrosc.* **2016**, *47*, 449−456.
(64) Tang, Y.; Yu, B. Coinage Metal (Bisfluorosulfonyl)imide Complexes: Preparation, Characterization, and Catalytic Applications. *Eur. J. Inorg. Chem.* **2020**, *2020*, 107−118.
(65) Ahrens, B.; Friedrichs, S.; Herbst-Irmer, R.; Jones, P. G. Hydrogen Bonding Networks in Bis(amine)gold(I) Complexes with Disulfonylamide Anions. *Eur. J. Inorg. Chem.* **2000**, *2000*, 2017−2029.
(66) Watkins, T.; Buttry, D. A. Determination of $Mg^{2+}$ Speciation in a TFSI Based Ionic Liquid With and Without Chelating Ethers Using Raman Spectroscopy. *J. Phys. Chem. B* **2015**, *119*, 7003−7014.
(67) Umebayashi, Y.; Mitsugi, T.; Fukuda, S.; Fujimori, T.; Fujii, K.; Kanzaki, R.; Takeuchi, M.; Ishiguro, S.-I. Lithium Ion Solvation in Room-Temperature Ionic Liquids Involving Bis-(trifluoromethanesulfonyl) Imide Anion Studied by Raman Spectroscopy and DFT Calculations. *J. Phys. Chem. B* **2007**, *111*, 13028−13032.
(68) Chai, J. D.; Head-Gordon, M. Long-range corrected hybrid density functionals with damped atom-atom dispersion corrections. *Phys. Chem. Chem. Phys.* **2008**, *10*, 6615−6620.
(69) Weigend, F.; Ahlrichs, R. Balanced basis sets of split valence, triple zeta valence and quadruple zeta valence quality for H to Rn: Design and assessment of accuracy. *Phys. Chem. Chem. Phys.* **2005**, *7*, 3297−3305.
(70) Marenich, A. V.; Cramer, C. J.; Truhlar, D. G. Universal Solvation Model Based on Solute Electron Density and on a Continuum Model of the Solvent Defined by the Bulk Dielectric Constant and Atomic Surface Tensions. *J. Phys. Chem. B* **2009**, *113*, 6378−6396.
(71) Bernales, V. S.; Marenich, A. V.; Contreras, R.; Cramer, C. J.; Truhlar, D. G. Quantum Mechanical Continuum Solvation Models for Ionic Liquids. *J. Phys. Chem. B* **2012**, *116*, 9122−9129.
(72) Xue, X.-S.; Wang, Y.; Yang, C.; Ji, P.; Cheng, J.-P. Toward Prediction of the Chemistry in Ionic Liquids: An Accurate Computation of Absolute pKa Values of Benzoic Acids and Benzenethiols. *J. Org. Chem.* **2015**, *80*, 8997−9006.
(73) Wang, Z.; Liu, W.; Li, B.; Liu, C.; Liu, S.; Su, W.; Ji, P. Bond Dissociation Free Energies in A Room-Temperature Ionic Liquid: Are Radical Species More Stable in an Ionic Liquid? *J. Org. Chem.* **2026**, *91*, 3475−3481.
(74) Frisch, M. J. et al. *Gaussian 16 Rev. A.03*, 2016.
(75) Cicco, A. D.; Aquilanti, G.; Minicucci, M.; Principi, E.; Novello, N.; Cognigni, A.; Olivi, L. Novel XAFS capabilities at ELETTRA synchrotron light source. *J. Phys. Conf. Ser.* **2009**, *190*, 012043.
(76) Filipponi, A.; Di Cicco, A.; Natoli, C. R. X-ray-absorption spectroscopy and *n*-body distribution functions in condensed matter. I. Theory. *Phys. Rev. B* **1995**, *52*, 15122−15134.
(77) Filipponi, A.; Di Cicco, A. X-ray-absorption spectroscopy and *n*-body distribution functions in condensed matter. II. Data analysis and applications. *Phys. Rev. B* **1995**, *52*, 15135−15149.
(78) Hedin, L.; Lundqvist, S. Effects of Electron-Electron and Electron-Phonon Interactions on the One-Electron States of Solids. *Solid State Phys.* **1970**, *23*, 1−181.
(79) Lassègues, J.-C.; Grondin, J.; Aupetit, C.; Johansson, P. Spectroscopic Identification of the Lithium Ion Transporting Species in LiTFSI-Doped Ionic Liquids. *J. Phys. Chem. A* **2009**, *113*, 305−314.
(80) Lassègues, J.-C.; Grondin, J.; Talaga, D. Lithium solvation in bis(trifluoromethanesulfonyl)imide-based ionic liquids. *Phys. Chem. Chem. Phys.* **2006**, *8*, 5629−5632.
(81) Lassègues, J. C.; Grondin, J.; Holomb, R.; Johansson, P. Raman and ab initio study of the conformational isomerism in the 1-ethyl-3-methyl-imidazolium bis(trifluoromethanesulfonyl)imide ionic liquid. *J. Raman Spectrosc.* **2007**, *38*, 551−558.
(82) Kesharwani, M. K.; Brauer, B.; Martin, J. M. L. Frequency and Zero-Point Vibrational Energy Scale Factors for Double-Hybrid Density Functionals (and Other Selected Methods): Can Anharmonic Force Fields Be Avoided? *J. Phys. Chem. A* **2015**, *119*, 1701−1714.
(83) Monti, D.; Jónsson, E.; Palacín, M. R.; Johansson, P. Ionic liquid based electrolytes for sodium-ion batteries: $Na^+$ solvation and ionic conductivity. *J. Power Sources* **2014**, *245*, 630−636.
(84) Stricker, M.; Oelkers, B.; Rosenau, C. P.; Sundermeyer, J. Copper(I) and Silver(I) Bis(trifluoromethanesulfonyl)imide and Their Interaction with an Arene, Diverse Olefins, and an $Tf_2N^-$Based Ionic Liquid. *Chem. Eur. J.* **2013**, *19*, 1042−1057.
(85) Gumaste, T.; Cooper, F. L.; Blakemore, J. D. Analysis of Bis(trifluoromethylsulfonyl)imide Interactions with Metal Cations Through a Chemical Informatics Approach. *Molecules* **2026**, *31*, 18.




https://doi.org/10.1021/acs.inorgchem.6c01404
*Inorg. Chem.* 2026, 65, 14023−14032